ELECTRONIC SUPPLEMENTARY INFORMATION

Interface Limited Charge Extraction and Recombination in Organic Photovoltaics

Abhishek Kumar[1], Girish Lakhwani[1], Einat Elmalem[2], Wilhelm T. S. Huck[2]^, Akshay Rao[1], Neil C. Greenham[1], Richard H. Friend[1]*

[1]Cavendish Laboratory, Department of Physics, University of Cambridge, J. J. Thomson Avenue, Cambridge CB3 0HE, U.K.

[2]Melville Laboratory for Polymer Synthesis, Department of Chemistry, University of Cambridge, Lensfield Road, Cambridge CB2 1EW, U.K.

* corresponding: rhf10@cam.ac.uk

Methods:

Material: PTB7 was purchased from 1-material Inc. and $PC_{70}BM$ was purchased from Nano-C. Both the chemicals were used as received. PEDOT:PSS was obtained from Heraeus (Clevios P VP AI 4083). $F(NSO_3)_2$ synthesis and characterization has been published elsewhere[1].

Film and device fabrication: The blend solution was prepared by dissolving PTB7 and $PC_{70}BM$ in the ratio 1:1.5 (w/w) in chlorobenzene: diiodooctane (96.7:3.3 v/v) solvent mixture. For optical characterization, thin films were made by spin coating the prepared solution on top of quartz substrates. For device fabrication, the ITO glass substrates were cleaned by sonicating it in acetone and isopropanol for 15 minutes successively, followed by treatment with oxygen plasma for 10 minutes. A 40nm thick layer of PEDOT:PSS was spin coated on top of the substrates, followed by annealing at 150^{o}C for 30 minutes under continuous nitrogen flow. The PEDOT:PSS coated substrate was quickly transferred inside nitrogen glovebox. A 100nm thick layer of prepared PTB7: $PC_{70}BM$ blend was spin coated on top of the PEDOT:PSS coated substrate. $F(NSO_3)_2$ was dissolved in polar solvent methanol and spin coated to make the interlayer film on top of the active layer. The thickness of the interlayer was controlled by changing the concentration of $F(NSO_3)_2$ in the solution and spin coating speed in the range of 2000-4000rpm. The thickness of the $F(NSO_3)_2$ interlayer was determined by AFM (NanoScope). All devices were completed by evaporation of 100 nm thick layer of metal (Aluminium for solar cell devices and Ag for single carrier devices) under high vacuum ($<10^{-6}$ mbar) through a 8-pixel shadow mask. The area of the photoactive layer within the devices was 4.5 mm^2. All devices were encapsulated and legged before testing to preserve its stability under spectroscopy measurements.

Device testing: The external quantum efficiency (EQE) of the devices was measured by a setup where a 100 W tungsten halogen lamp, dispersed through a monochromator, was used as the light source and a Keithley 237 source meter unit (SMU) was used to measure the short circuit current at various wavelengths. The incident light intensity was continuously monitored during experiments by using a reference photodiode calibrated by a Hamamatsu S8746-01 calibrated photodiode. Current–voltage (*J-V*) characteristics were measured under 100 mW cm^{-2} AM 1.5 conditions using an ABET Sun2000 solar simulator calibrated to a silicon reference cell, correcting for spectral mismatch. The short-circuit current density was also corrected for illumination area masking. Both the dark and light current-voltage characteristics were measured using the Keithley 237 SMU.

Spectroscopy: For TA measurements, the frequency-doubled output (532 nm) of a q-switched Nd:YVO4 laser (Advanced Optical Technologies AOT-YVO-25QSPX) was employed as the pump to allow for the use of electronic delay. The transmission of the sample was probed using broadband (950-1100 nm) output of a home-built non-collinear optical parametric amplifier (NOPA), which was pumped with ultrafast pulses (90fs) derived from the output of a kHz regenerative amplifier (Spectra-Physics Solstice). The probe beam was split to provide a reference signal not affected by the pump to mitigate the effect of laser fluctuations. The pump and probe beam were focused on the same spot on the active area of the device and the reference beam was focused on a spot of the same device. Probe and reference beams pass through the active device and are reflected off the back electrode. The reflected probe and reference beams are collected and dispersed in a spectrometer (Andor, Shamrock SR-303i) and detected using a pair of 16-bit 1024-pixel linear image sensors (Hamamatsu), which were driven and read out at 1 kHz by a custom-built board from Stresing Entwicklunsburo. The signal between 1000-1100nm was averaged to produce the kinetic traces shown in figure 3a.

Transient photocurrent decay kinetics was measured by a setup where high-brightness 525 nm green LED (Kingbright, L-7104VGC-H) was used as the step pulse source to excite the devices (without any background illumination) and to reach steady state. A Hewlett Packard (HP) 8116A pulse/ function generator was used as the power supply for the green LED. As steady state condition reached, the pulse was stopped and the transient photocurrent decay dynamics was recorded with an Agilent DSO6052A digitizing oscilloscope with input impedance of 50 Ω.

Experimental data:

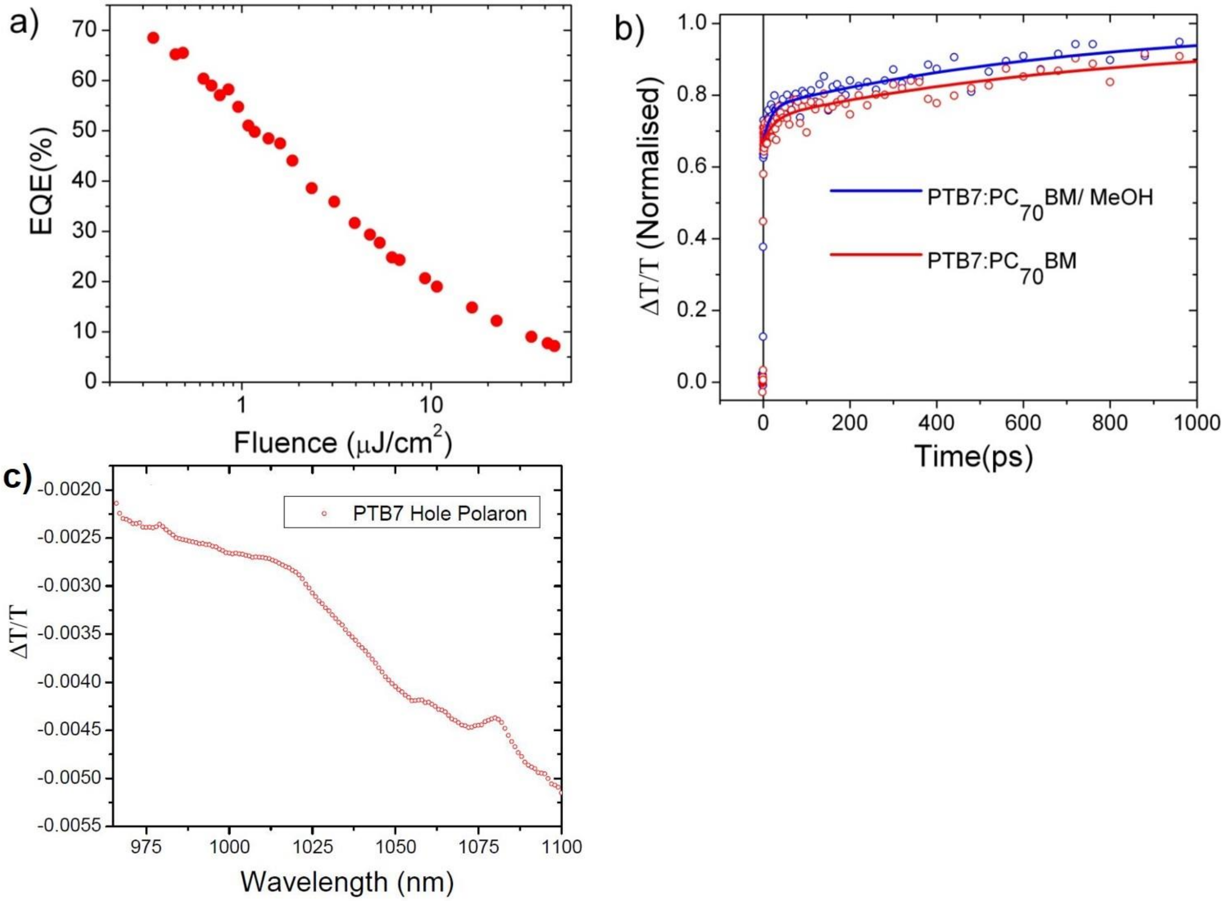

Figure S1: (a) Device EQE measured as a function of pulse intensity for a 600ps 532nm laser pulse used in the transient absorption measurement. At high pulse intensity the EQE falls dramatically indicating the presence of bimolecular annihilation pathways. In order to study the physics of devices in conditions relevant to that under solar illumination we perform TA measurements at low fluences (0.5μJ/cm^2). At this fluence the device EQE is similar to that measured under CW conditions (Figure 2(b)) **(b)** Ultrafast transient absorption measurements on a pristine film of PTB7:PC$_{70}$BM pristine film and a methanol treated film. The polaron signal is monitored between 1050-1150nm. The majority of the charges are generated on ultrafast timescales, with a small fraction of charges generated on ps time scales following exciton diffusion. No significant difference in charge generation times were observed indicating that the active layer morphology is not significantly changed via the methanol treatment. This is in contrast to the affects of thermal annealing. **(c)** TA spectrum of the hole polaron in a PTB7:PC$_{70}$BM device, measured 5ns after photoexcitation. The hole polaron spectra matches with that of PTB7 reported in SI ref 2. The spectrum is seen to peak beyond 1100nm. The spectra range (950-1100nm) is determined by the bandwidth of the broadband near-IR NOPA as described in the Methods. The range from 1000-1100nm are averaged to obtain the kinetics shown in Figure 3(a). We note that the spectrum shown in S1(c) is taken at a high fluence (5μJ/cm^2) in order to show the shape of the spectrum clearly. Measurements shown in Figure 3(a) are taken at lower fluence (0.5μJ/cm^2) as described above.

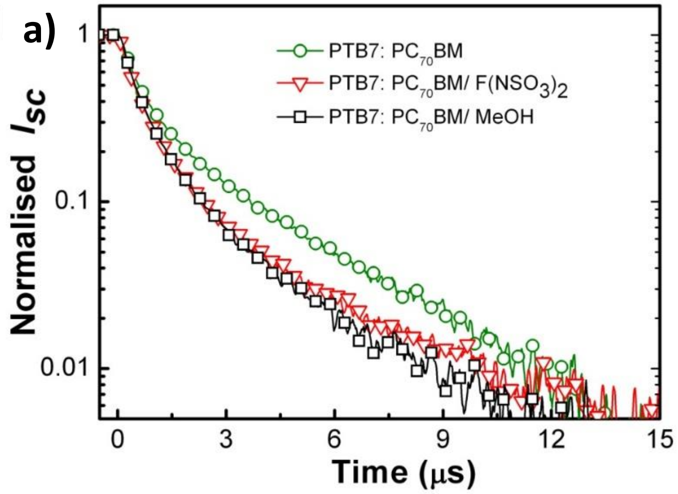

Figure S2: (a) Normalized transient photocurrent decay kinetics of devices measured under short-circuit conditions for a reference PTB7:PC$_{70}$BM device with no modification (**Green circles**); a device modified with 2nm F(NSO$_3$)$_2$ **(Red triangles**); and a device modified with methanol **(Black squares**). The devices were excited with a 525nm light-emitting diode.

S3(a) plots the J_{SC} *vs* illumination intensity of the reference and the modified devices. The J_{SC} exhibited a power-law dependence,

$$J_{\mathrm{SC}} \propto I^{\alpha} \tag{S1}$$

where I is the illumination intensity and α is the coefficient of the power law. The value of α is 0.89 for reference PTB7:PC_{70}BM devices and 0.90 for PTB7:PC_{70}BM/F$(NSO_3)_2$-2 nm devices. In the literature, power law correlation has been reported for polymer-fullerene OPVs [3-5]. The values obtained for our devices are close to 0.9, similar to those reported for common polymer-fullerene systems [3,4].

Figure S3(b) plots the V_{OC} of the same devices as a function of illumination intensity. In literature, V_{OC} *vs* illumination intensity measurement has been used to investigate the nature of the recombination mechanism inside the active layer [6,7]. At V_{OC}, there is no net current flowing out of the device hence the generation and recombination must balance to establish a quasi-steady state. V_{OC} follows a correlation with the charge generation as,

$$V_{\mathrm{oc}} \propto \eta \frac{kT}{q} \ln(\frac{J_p}{J_s} + 1) \tag{S2}$$

where q is the elementary charge; k is Boltzmann's constant; T is the absolute temperature, J_P is the photogenerated current density; and J_S is saturated current density (under reverse bias). η is ideality factor which indicates how close the device is to an ideal diode. The η calculated for the PTB7:PC_{70}BM and PTB7:PC_{70}BM/F$(NSO_3)_2$ -2nm devices were 0.90 and 1.29, respectively. For an ideal diode the ideality factor should be 1 however the ideality factor for practical diodes are not 1. The deviation in the value of the ideality factor from 1 is usually attributed to bimolecular recombination processes [5].

At 1mW/cm^2, the difference in V_{OC} between the baseline and interfacial treated device is 50mV. At low intensity, the device is operating near dark condition with relatively negligible bimolecular recombination. This increase is due to the overall decrease in $J_{inj}(V)$, requiring an increase in voltage under 1mW/cm^2 illumination in order for injection and extraction to balance at open-circuit condition. However, as the illumination intensity was increased the interfacial treated devices demonstrated further 50mV increase in V_{OC}. At higher illumination intensity, the bimolecular recombination became a dominant process in the device. The improved extraction from the interfacial treated devices suppresses the bimolecular recombination.

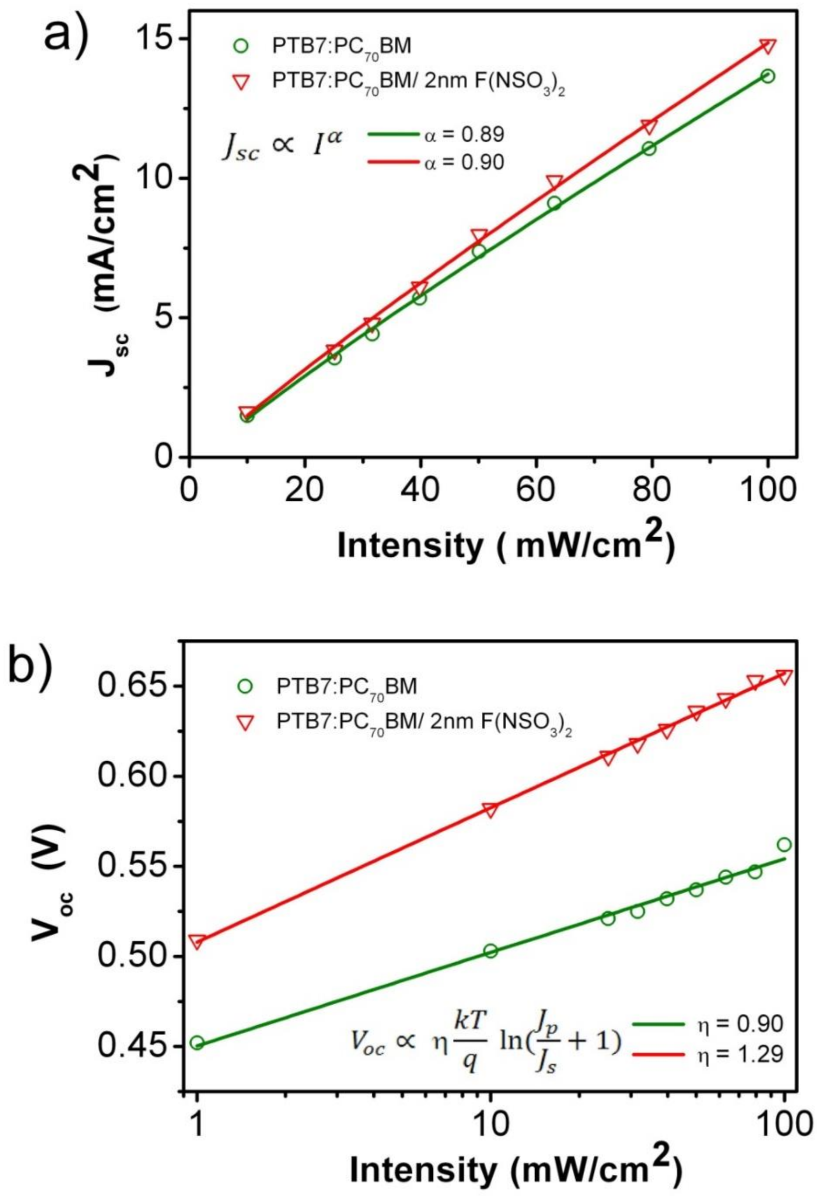

Figure S3: (a) Short circuit current density measured with increasing illumination intensity for reference PTB7:PC$_{70}$BM device with no modification (Green circles); device modified with 2nm thin F(NSO$_3$)$_2$ (red triangles) **(b)** the evolution of V_{OC} of same devices with increasing illumination intensity.

The swelling of the PEDOT:PSS/PTB7:$PC_{70}BM$ film was estimated by reflectometry measurements of the PTB7:$PC_{70}BM$ film on top of a reflective Si substrate. The film was kept in closed chamber with ambient atmosphere and the reflectance was measured using a split fibre to illuminate the sample with a halogen lamp and collect the reflected light with a diode array spectrometer. An atmosphere of nitrogen with 95% saturation of methanol vapour, which was controlled by using digital massflow controllers, introduced into the chamber as described elsewhere[8]. Reflectometry is used to measure the thickness of the films by evaluating the interference pattern. Since the PTB7:$PC_{70}BM$ shows a strong absorption within the range we use this method rather as a simple qualitative way to observe film swelling. No changes upon solvent vapour exposure were observed with a pristine PTB7:$PC_{70}BM$ film (S4 (b)), indicating no solvent uptake. In case of the underlying PEDOT:PSS film, swelling could be observed. The reflectance spectra of the PTB7:$PC_{70}BM$ /PEDOT:PSS film changed due to the swelling (S4 (a)). After 240s, the supply of the methanol vapour was stopped and sample box was purged with dry nitrogen. The reflectance of the PTB7:$PC_{70}BM$ /PEDOT:PSS film recovered back to the original value.

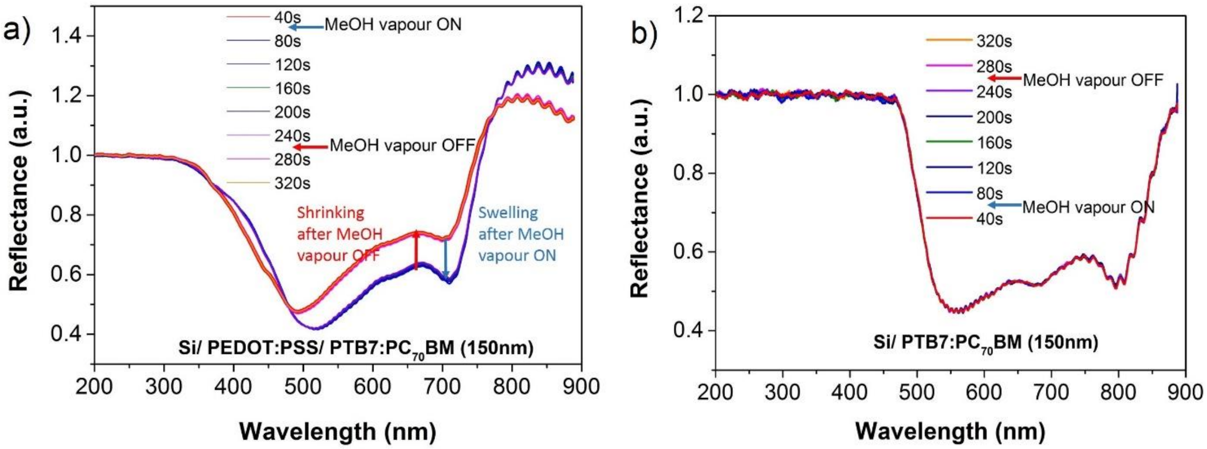

Figure S4: The reflectometry measurements of (a) PEDOT:PSS/ PTB7:$PC_{70}BM$ (b) PTB7:$PC_{70}BM$ film.

The thickness of CPE interlayer plays an important role in the charge extraction process (Figure S5). These classes of ionic polymers are known to have poor transport property [9,10]. On increasing the thickness of interlayer from 2nm to 14nm the poor transport property of the ZCPE plays a dominant role and it suppresses the *J*sc. The poly(9,9-dioctylfluorene) based ZCPE i.e. $F(NSO_3)_2$ has LUMO level at -2.6eV. The higher LUMO for $F(NSO_3)_2$ could also block the electron extraction from $PC_{70}BM$ to Al electrode, when a 14nm layer of $F(NSO_3)_2$ was inserted between them. Similar decrease in the *J*sc was also observed by Chang et al.[11] when they increased the thickness of CPE interlayer by increasing its concentration in the methanol solution. This blocking effect in the PTB7:$PC_{70}BM$ devices with 14nm thick $F(NSO_3)_2$ could lead to the recombination losses. Chang et al.[11] has reported that the stability of the solar cell devices improved after treatment with CPE.

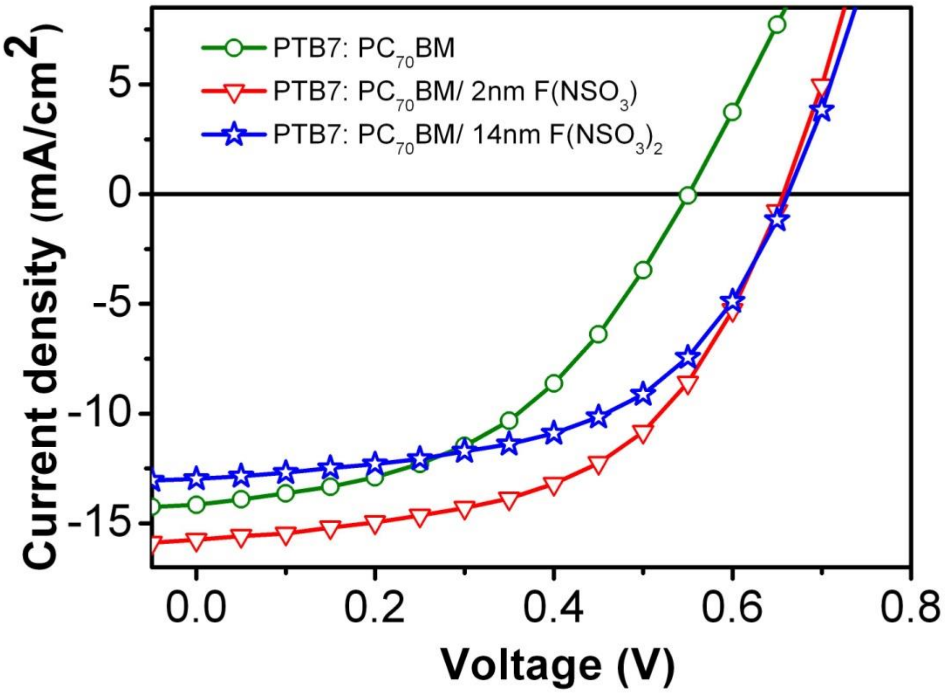

Figure S5: The *J*-*V* characteristics under AM 1.5G for PTB7:$PC_{70}BM$ devices with no modification (Green circles) as reference, modified with thin interlayer (2nm) of $F(NSO_3)_2$ (Red triangle), and when modified with thick interlayer (14nm) of $F(NSO_3)_2$ (Blue star).

We note that direct treatment of the PEDOT:PSS layer with methanol followed by active layer deposition does not lead to an increase in V_{OC} and instead leads to a loss of J_{SC} (S6). This is consistent with TA measurements (S8) that show slow extraction in these devices and increased recombination on shorter time scales. It is possible that this drop in performance is caused by the degradation of the PEDOT:PSS, which is soluble in methanol, leading to a poor interface with the photoactive-layer. Thus the formation of the PEDOT:PSS/photoactive-layer interface, before methanol treatment, is necessary to bring about an increase in V_{OC}.

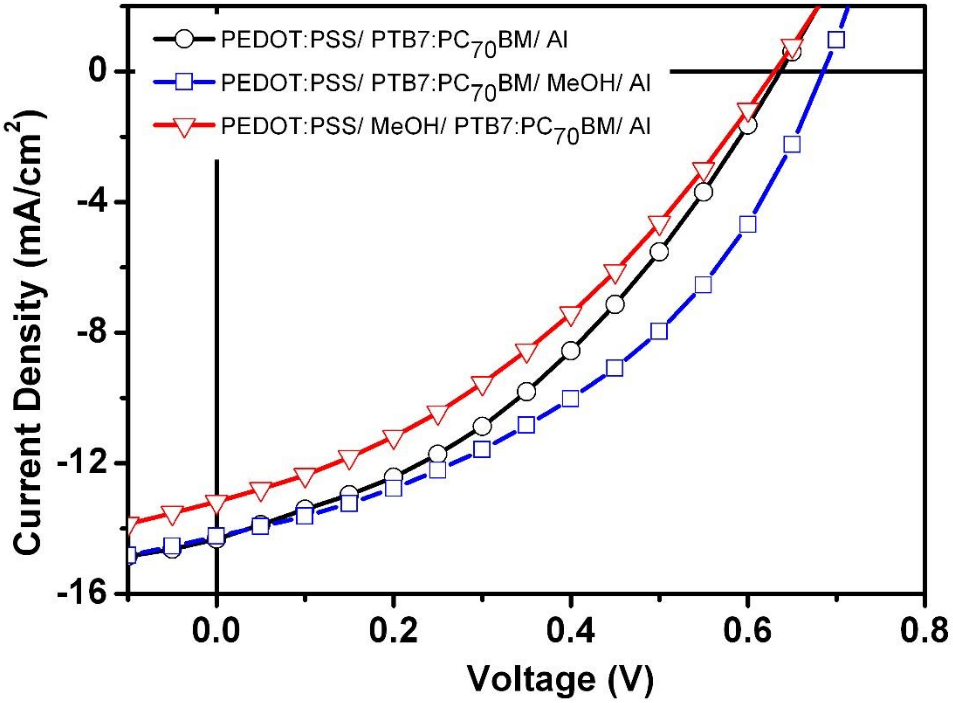

Figure S6: *J-V* characteristics under AM 1.5G 1-sun illumination for PTB7:$PC_{70}BM$ devices with no modification (Black circles) as reference, modified with methanol before active-layer deposition (Red triangle), and after active-layer deposition (Blue square). Modification with methanol before active-layer deposition leads to a drop in J_{SC} and no change in V_{OC}.

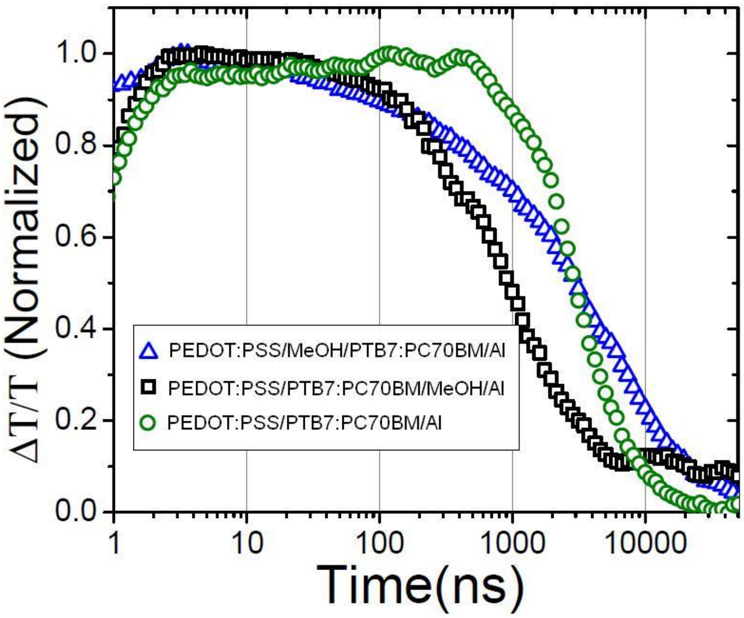

Figure S7: Normalised kinetics for holes in operating devices measured in-situ via TA spectroscopy at 0 V bias applied bias for: a reference PTB7:PC_{70}BM device with no modification (Green circles); a device modified with methanol before depositing PTB7:PC_{70}BM (Blue triangle) and a device modified with methanol after depositing PTB7:PC_{70}BM (Black squares). The device modified with methanol before depositing PTB7:PC_{70}BM does not show the fast extraction shown by the device modified with methanol after depositing PTB7:PC_{70}BM, and rather shows increased recombination at times before 1μs. This is consistent with the lower J_{SC} in such devices, as shown in S6.

Table T1: Table listing the average value of key parameters, V_{OC}, J_{SC}, fill factor (FF) and power conversion efficiency. The device parameters are average of 4 devices.

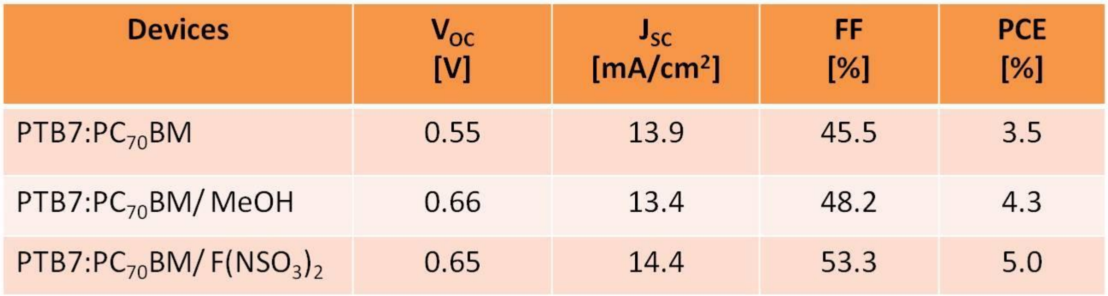

Devices	V_{OC} [V]	J_{SC} [mA/cm^2]	FF [%]	PCE [%]
PTB7:PC$_{70}$BM	0.55	13.9	45.5	3.5
PTB7:PC$_{70}$BM/ MeOH	0.66	13.4	48.2	4.3
PTB7:PC$_{70}$BM/ F(NSO$_3$)$_2$	0.65	14.4	53.3	5.0

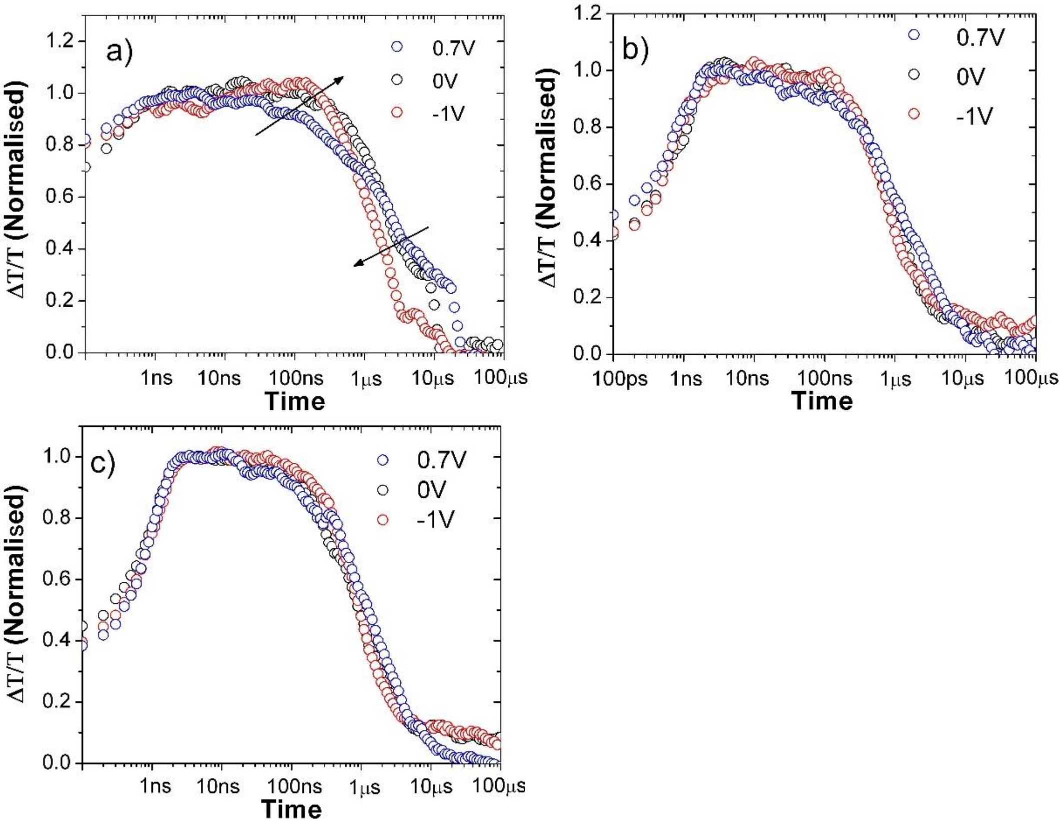

Figure S8: Normalised kinetics of the holes in the operating devices measured *in-situ* via TA spectroscopy at a series of applied bias in (a) reference PTB7:PC$_{70}$BM device with no modification, (b) device modified with F(NSO$_3$)$_2$, and (c) device modified with methanol treatment.

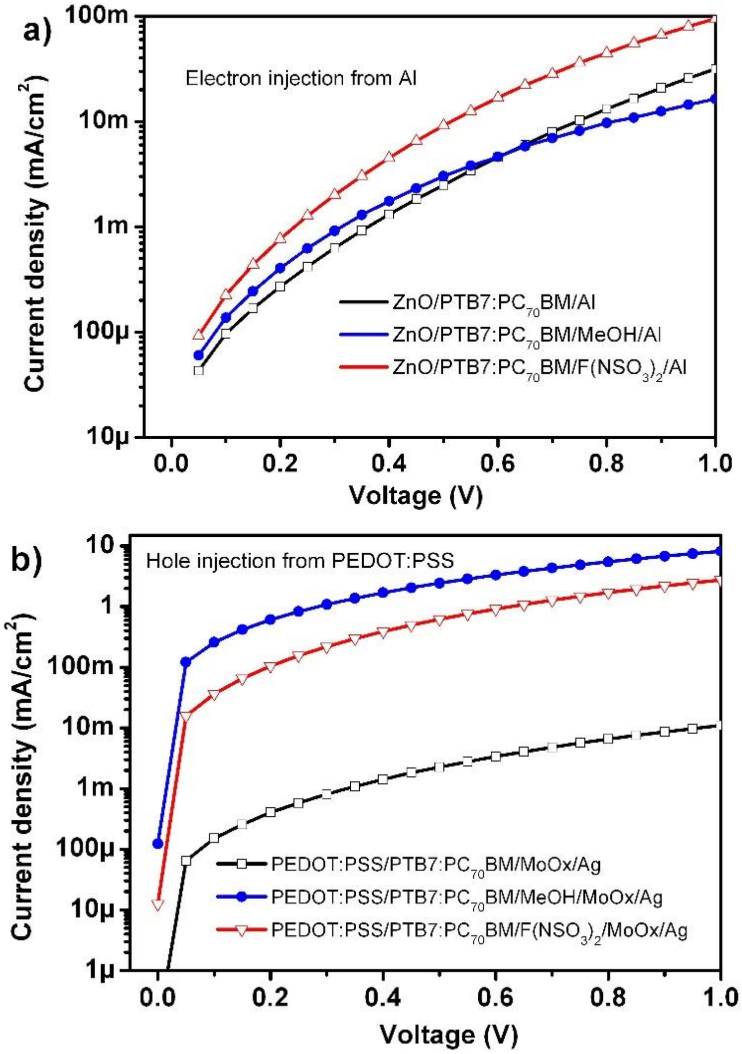

Figure S9: Dark *J-V* characteristics for (a) electron only and (b) hole only, PTB7:PC$_{70}$BM devices with no modification (Black squares), modified with methanol (Blue circles), and modified with 2nm F(NSO$_3$)$_2$ (Red triangles).

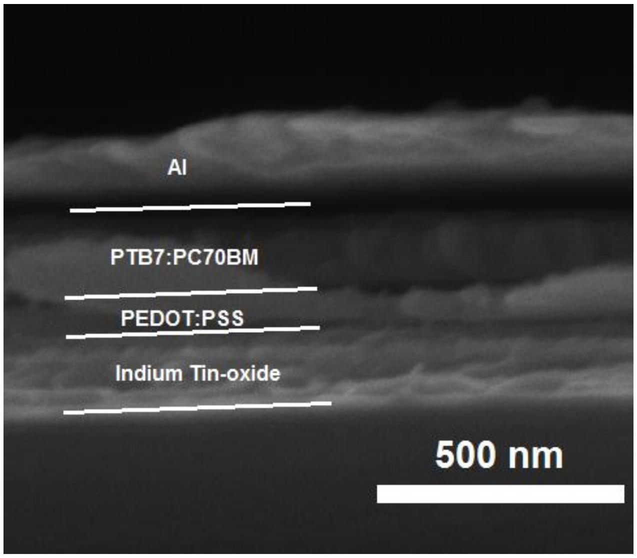

Figure S10: Scanning electron micrograph of the ITO/PEDOT:PSS/PTB7:PC_{70}BM/Al device.

1. J. Fang, B. H. Wallikewitz, F. Gao, G. Tu, C. Muller, G. Pace, R. H. Friend, W. T. S. Huck, *Journal of the American Chemical Society* **2011**, *133*, 683.

2. M. P. Nikiforov, B. Lai, W. Chen, S. Chen, R. D. Schaller, J. Strzalka, J. Maserb, S. B. Darling, *Energy and Environmental Science*., **2013**, 6, 1513.

3. L. J. A. Koster, V. D. Mihailetchi, H. Xie, P. W. M. Blom, *Applied Physics Letters* **2005**, *87*, 203502.

4. L. J. A. Koster, V. D. Mihailetchi, P. W. M. Blom, *Applied Physics Letters* **2006**, *88*, 052104.

5. G. A. H. Wetzelaer, M. Kuik, M. Lenes, P. W. M. Blom, *Applied Physics Letters* **2011**, *99*, 153506.

6. M. M. Mandoc, F. B. Kooistra, J. C. Hummelen, B. de Boer, P. W. M. Blom, *Applied Physics Letters* **2007**, *91*, 263505.

7. M. M. Mandoc, W. Veurman, L. J. A. Koster, B. de Boer, P. W. M. Blom, *Advanced Functional Materials* **2007**, *17*, 2167.

8. S. Huttner, M. Sommer, A. Chiche, G. Krausch, U. Steiner, M. Thelakkat, *Soft Matter* **2009**, *5*, 4206.

9. C. V. Hoven, A. Garcia, G. C. Bazan, T.-Q. Nguyen, *Advanced Materials* **2008**, *20*, 3793.

10. A. Garcia, R. C. Bakus Ii, P. Zalar, C. V. Hoven, J. Z. Brzezinski, T.-Q. Nguyen, *Journal of the American Chemical Society* **2011**, *133*, 2492.

11. Y.-M. Chang, R. Zhu, E. Richard, C.-C. Chen, G. Li, Y. Yang, *Advanced Functional Materials* **2012**, *22*, 3284.